

# Event distributions of polymer translocation

R. P. Linna and K. Kaski

*Department of Biomedical Engineering and Computational Science,  
Aalto University, P.O. Box 12200, FI-00076 Aalto, Finland*

We present event distributions for the polymer translocation obtained by extensive Langevin dynamics simulations. Such distributions have not been reported previously and they provide new understanding of the stochastic characteristics of the process. We extract at a high length scale resolution distributions of polymer segments that continuously traverse through a nanoscale pore. The obtained log-normal distributions together with the characteristics of polymer translocation suggest that it is describable as a multiplicative stochastic process. In spite of its clear out-of-equilibrium nature the forced translocation is surprisingly similar to the unforced case. We find forms for the distributions almost unaltered with a common cut-off length. We show that the individual short-segment and short-time movements inside the pore give the scaling relations  $\tau \sim N^\alpha$  and  $\tau \sim f^{-\beta}$  for the polymer translocation.

PACS numbers: 87.15.A-, 82.35.Lr, 82.37.-j

## I. INTRODUCTION

Polymer translocation through a nano-scale pore has been under intensive research since the experimental study by Kasianowicz *et al.* [1] and the first theoretical treatment by Sung and Park [2] and the related study by Muthukumar [3]. The important treatment in [4, 5] set the valid limits for the scaling exponents obtained for the unforced and forced translocation. The highly non-equilibrium nature of the process was captured in the first analytical treatment based on the tension propagation present in the forced translocation by Sakaue [6]. Broadly speaking, the present theoretical translocation research is spanned between these few cornerstones.

We have previously shown that the forced polymer translocation takes place out of equilibrium and is mainly determined by the balance between the driving pore force and the drag force exerted on the polymer on the *cis* side [7, 8]. The drag force magnitude was shown to change with the tension propagation, which shows as an increase in the number of moving polymer beads  $N_m$  on the *cis* side. The drag force was shown to consequently decrease with  $N_m$  as the polymer translocates to the *trans* side. The polymer crowding on the *trans* side was shown to modify this dynamics and be enhanced by increasing the pore force. The crowding in turn increases the scaling exponent  $\alpha$  in  $\tau \sim N^\alpha$  where  $\tau$  is the translocation time and  $N$  the number of polymer beads, *i.e.* the polymer length [7, 8]. We also showed that  $\alpha$  decreases with increasing the pore friction [9]. Our description of the process is very closely aligned with Sakaue's analytical treatment that has been adopted and expanded *e.g.* in [10]. Sakaue's treatment and the characteristics described above have been incorporated in a coarse-grained model in [11].

The coarse-grained description of the forced polymer translocation outlined above says very little about the stochastic nature of the process. The force balance and tension propagation fall within the realm of classical mechanics. Although they give the correct average characteristics of the forced polymer translocation, for example the question of how frequently the translocating polymer stops and reverses its direction and how long segments typically pass through the pore

“in one go” and how long such transitions take remain unanswered. Questions such as these have relevance for implementing DNA sequencing. The force balance and tension propagation framework can outline the force dependence of the observed scaling of the translocation time  $\tau$  with the polymer length  $N$  but cannot describe how this scaling comes about in the first place. In this paper our motivation is to characterize the stochastic nature of the polymer translocation and the origin of the scaling by collecting data on the individual transitions of polymer segments.

A fundamental question is how the forced translocation differs stochastically from the unforced process. The forced polymer translocation is a highly non-equilibrium process even for a modest driving pore force. From the pore outward on both the *cis* and the *trans* side an increasing portion of the polymer is lifted out of thermal equilibrium in the course of translocation [7, 8, 12]. The correlations along the polymer contour increase due to the polymer being driven out of equilibrium. Hence, it is natural to expect that applying the pore force may alter the obtained distributions describing the transfer of polymer segments through the pore. As we will show, these distributions also shed light on the way the observed scaling relations emerge. We have previously found that the waiting-time distribution, *i.e.* the numbers of transitions  $n$  that take a time  $\Delta t$  plotted as a function of  $\Delta t$ ,  $n(\Delta t)$ , obey closely the Poisson distribution [12]. The events, *i.e.* the transitions of individual segments were registered with the resolution of a polymer bond length  $b$ . It is clear that the polymer translocation for which the translocation time  $\tau$  scales with the polymer length  $N$  cannot be a Poissonian process. One is then naturally led to presume that the polymer translocation shows additional correlations if observed at smaller length scales than  $b$ .

The outline of the paper is as follows: In Section II the computational model and its relation to experiments is explained. In Subsection III A we define the events that we register from the simulated polymer translocations. The multiplicative stochastic process is defined and the polymer translocation as such a process described in Subsection III B. The results are reported and discussed in the remaining parts of Section III. Finally, in Section IV we summarize the main conclu-

sions based on our findings.

## II. THE COMPUTATIONAL MODEL

### A. The polymer model

We use the standard bead-spring chain as a coarse-grained model for the polymer. Here, adjacent monomers are connected with anharmonic springs, described by the finitely extensible nonlinear elastic (FENE) potential

$$U_F = -\frac{K}{2}R^2 \ln\left(1 - \frac{r^2}{R^2}\right), \quad (1)$$

where  $r$  is the length of an effective bond and  $R = 1.5\sigma$  is the maximum bond length. The shifted Lennard-Jones (LJ) potential

$$U_{LJ} = 4\epsilon \left[ \left(\frac{\sigma}{r}\right)^{12} - \left(\frac{\sigma}{r}\right)^6 + \frac{1}{4} \right], \quad r \leq 2^{1/6}, \quad (2)$$

is applied between all beads of distance  $r$  apart. The parameter values were chosen as  $\epsilon = 1.0$ ,  $\sigma = 1.0$  and  $K = 30/\sigma^2$ . As there is no attractive part in the used LJ potential, the model is for a polymer in a good solvent. We apply no bending potential, rendering the polymer as a freely-jointed chain (FJC), instead of a worm-like chain (WLC). We have previously shown that the difference of the two models when simulating polymer elasticity in mechanical stretching or in flow is insignificant [13].

### B. The dynamics

The dynamics of the polymer translocation was simulated using Ermak's implementation of Brownian dynamics [14]. Accordingly, the time derivative of the momentum of the polymer bead  $i$  is given by

$$\dot{\mathbf{p}}_i(t) = -\xi \mathbf{p}_i(t) + \eta_i(t) + f(\mathbf{r}_i), \quad (3)$$

where  $\xi$ ,  $\mathbf{p}_i(t)$ ,  $\eta_i(t)$ , and  $f(\mathbf{r}_i)$  are the friction constant, momentum, random force of the bead  $i$ , and external driving force, respectively. When applied,  $f(\mathbf{r}_i)$  is constant and exerted only inside the pore. Velocity Verlet was applied in the time integration [15]. In the present study the parameter values in reduced units [16] were as follows:  $\xi = 0.5$  and  $\eta_i(t)$  is related to  $\xi$  by the fluctuation-dissipation theorem. The mass of a polymer bead is  $m = 16$ . The time step used in the numerical integration of equations of motion was  $\delta t = 0.001$ . Partly due to the out-of-equilibrium nature of driven translocation, changing either  $\xi$  or  $m$  changes the obtained scaling of the translocation time with the number of beads,  $\tau \sim N^\alpha$  [9].

### C. The wall and the pore

The wall comprises two aligned surfaces the distance  $l = 3b$  apart, where  $b = 1$  is the Kuhn length for the model poly-

mer.  $l$  is thus the length of the pore. No-slip boundary conditions applied on the polymer beads hitting the surfaces prevent them from entering the wall. The pore is modelled as a cylindrical potential whose center axis is perpendicular to the wall and extends through it. The pore diameter is  $1.2\sigma$ . Inside the pore, the cylindrically symmetric damped harmonic potential  $U_h$  pulls the beads toward the pore axis with force

$$f_h = -\nabla U_h = -kr_p - cv_p, \quad (4)$$

where  $k = 100$ ,  $c = 1$ ,  $r_p$  is the distance of a polymer bead from the pore axis, and  $v_p$  is its velocity component perpendicular to the axis. As mentioned in Subsection II B, the pore force  $f(\mathbf{r}_i)$  in Eq. (3) is exerted only inside the pore in the case of forced translocation. To prevent the pore force from fluctuating with the changing number (2 or 3) of polymer beads inside the pore we calculate the exact fraction of the polymer inside the pore and adjust the force magnitude applied on each bead inside the pore so that the pore exerts a constant force per polymer length.

There is no explicit adhesion between the polymer and the pore in our model. While adhesion is of importance in the DNA translocation experiments, see *e.g.* [17], here we want to characterize the basic translocation process prior to embarking on the effects of relevant additional interactions. The transitions and pauses of the polymer segments inside the pore hence result from the changes in the force exerted on these segments inside the pore. These changes in the force, in turn, reflect the conformational changes of the polymer segments outside the pore and their changing interactions with the Brownian heat baths on the *cis* and *trans* sides of the wall.

### D. Relation to experiments

In order to relate the computational force to a physical force inside a pore in experiments we need to relate the energy and length scale in our model to the physical energy and length scale. In our reduced units  $kT = 1$  corresponds to  $k_B \bar{T}$ , where  $k_B$  is the Boltzmann constant, and the physical temperature  $\bar{T}$  is taken to be 300 K. The correspondence between computational and physical length scales can be established by taking the polymer bond length  $b$  as the Kuhn length for the physical polymer. In SI units the bond length for our FJC model polymer can be obtained as  $\bar{b} = 2\lambda_p$ , where  $\lambda_p$  is the persistence length, 40 Å for a ssDNA [18]. The pore force per bond length in SI units,  $\bar{f}_{tot}$ , is then obtained from the dimensionless pore force per bond segment,  $f$ , by relating  $\bar{f}\bar{b}/k_B\bar{T} = fb/kT$ . The effective pore force per bond of  $f = 1$  thus corresponds to  $\bar{f} = 0.52$  pN per Kuhn length for a ssDNA. Since  $l = 3b$ ,  $f = 1$  corresponds to the total pore force  $\bar{f}_{tot} = 1.56$  pN. If one uses Manning condensation leading to drastic charge reduction [19, 20] to relate this to experiments, in the  $\alpha$ -HL pore a typical pore potential of  $\approx 120$  mV would correspond to  $\bar{f}_{tot} \approx 5$  pN. In the light of recent computer simulations the reduction of the effective force inside the  $\alpha$ -HL pore is not predominantly caused by the Manning condensation but by electro-osmotic flow that

is driven by the motion of counterions along the surface of DNA [21, 22]. However, experiments indicate that the estimate based on Manning condensation is in the right order of magnitude [23].

### III. RESULTS: EVENTS OBSERVED WITH HIGH RESOLUTION

Traditionally, an event in a translocation simulation is defined as a change of the polymer bead at a reference position, here the pore opening on the *trans* side. In order to discern correlations at a finer scale than  $b$  we have implemented in our model the possibility to register polymer segment motion inside the pore with the resolution  $b/10$ . In addition, we redefine the event as a polymer segment traversed in one direction inside the pore. The event-related distributions were extracted from at least 1000 individual translocation runs for each pore force. The runs ending in the polymers translocating to the *trans* side and the ones where they slid back to the *cis* side were identified. Distributions were determined for all runs and the *trans* and *cis* cases, separately.

#### A. Numbers of events vs traversed segment lengths

First, we define the event as a polymer segment  $\Delta s$  that traverses in either direction inside the pore without pausing. We sample these events at constant time intervals  $t_{int}$ . Already using this somewhat limited definition for an event reveals a log-normal distribution for the number of events  $n_E$  vs  $\Delta s$ . In Fig. 1(a) we show distributions  $n_E(\Delta s)$  for different pore force magnitudes. The distributions for motion toward *cis* and *trans* are identical for unforced translocation. Increasing the pore force  $f$  these distributions deviate due to the increasing proportion of events toward *trans*.

The total time  $\tau$  it takes a polymer to translocate consists of forward and backward motion and pauses. In order to find how the scaling law  $\tau \sim N^\alpha$  emerges we have to include the pauses in the definition of the events and register events without the time limit introduced by the time interval  $t_{int}$ . Accordingly, we define an event to be terminated only when the direction of the motion is reversed. The characteristics are the same as with the first event definition, only the distributions become wider. To compare the forms of the distributions we normalize them with the maximum number of events,  $\hat{n}_e = n_e/n_{max}$ . These normalized log-binned distributions are shown in Fig. 1(b). For clarity, the separated distributions toward *cis* are shown only for the events defined in the first way.

#### B. Log-normal distribution and multiplicative stochastic processes

The obtained log-normal distributions suggest that the polymer translocation is largely dominated by the underlying *multiplicative* stochastic process. For such a process the prob-

ability of an event  $P_r^{(m)}$  composed of the succession of  $m$  independent events with the probabilities  $p_i$  ( $1 \leq i \leq m$ ) is given by the product of these independent random variables  $P_r^{(m)} = \prod_{i=1}^m p_i$ , so that  $\log P_r^{(m)} = \sum_{i=1}^m \log p_i$ . With  $m$  large,  $\log P_r^{(m)}$  becomes a normal and, hence,  $P_r^{(m)}$  a log-normal distribution due to the central limit theorem [24].

In the case of polymer translocation this multiplicativity arises naturally, since we observe traversed polymer segments  $\Delta s_n$ . Here,  $n$  indexes the registered segments. The traversed segments  $\Delta s_n$  toward *trans* result from  $m$  consecutive transitions of distance  $s_i$  toward *trans*. An analogous statement applies, of course, for transitions toward *cis*. Denoting the probabilities of these individual transitions as  $p_i$  ( $1 \leq i \leq m$ ), we see that the probability of  $m$  such consecutive transitions is  $P_r^{(m)} = \prod_{i=1}^m p_i$ . Hence, the polymer translocation is seen to be of the simplest type of a multiplicative process. Since the traversed segments  $\Delta s_n = m s_i$ , the probability distribution  $P(\Delta s_n)$  is of the same form as  $P_r^{(m)}$ . Taking the continuum limit, the enumerable set  $\{\Delta s_n\}$  is replaced by the continuous variable  $\Delta s$ . In this limit  $P(\Delta s)$  is log-normal due to the central limit theorem. In what follows we drop the subscript  $n$  and use the symbol  $\Delta s$  to denote the lengths of the traversed segments registered with resolution  $b/10$ .

There are subtleties in applying the central limit theorem to multiplicative processes, see [25]. These are related to the effect of rare events. In our case these correspond to large  $m$ , or  $\Delta s$ . As we will see, the translocation is dominated by short  $\Delta s$  events, so applying the central limit theorem is valid and the obtained log-normal distributions have the natural explanation described above.

The probabilities  $p_i$  appear independently but are dependent on the stage of the translocation process. Transition toward *trans* gets more probable toward the end of the translocation process when the majority of the polymer is already translocated. Also the crowding of the polymer segments at large pore force changes this probability by different amounts at different stages of translocation [7]. This differing of  $p_i$ 's at different stages of the process is characteristic for multiplicative stochastic processes, see *e.g.* [26]. Due to the additional correlations in fluctuations multiplicative stochastic processes are typically highly non-equilibrium processes [26, 27], which we have shown to be the case for the polymer translocation [7, 8].

The observed traversed polymer segments  $\Delta s$  consist of successive individual transitions  $s_i$  measured with resolution  $b/10$ . The transitions were seen to be slow enough that the registered  $s_i = \pm b/10$ . We obtain distributions of the log-normal form

$$P(\Delta s) \sim \frac{1}{\Delta s} \exp[-\ln(\Delta s/\Delta s_0)^2/2\sigma^2], \quad (5)$$

where  $\Delta s_0$  is the characteristic scale and  $\sigma$  the standard deviation of the variable  $\ln \Delta s$ , see *e.g.* [28]. To further confirm that we are indeed sampling events from a distribution resulting from a multiplicative stochastic process we also registered each successive transition at times  $i$  and collected distributions such that even successive transitions of different lengths in



the same direction were identified as separate events. Again, clean log-normal distributions resulted.

The forms of the *trans* distributions are seen to become wider with increasing pore force  $f$ . This is due to the increased proportion of long-segment motion at larger  $f$ . In accordance, the *cis* distributions become narrower with increasing  $f$ . However, the distributions vary fairly little with  $f$ . Especially surprising is the small difference between the distributions for unforced and forced translocation in spite of the fact that forced translocation already at weak pore force was seen to be governed by a non-equilibrium force balance condition [7, 8]. In what follows, we show results for distributions obtained using the latter event definition.

### C. Numbers of events vs event times

Next, we look at the distribution of events in terms of event times  $\Delta t$ . Fig. 2 shows the event-time distributions of the segments traversed toward *trans* and *cis* for  $f = 1$  and  $N \in \{50, 100, 200\}$ . The number of events toward *trans* decays as  $n_E \sim e^{-A\Delta t}$ . The transfer times of the events toward *cis* obey  $n_E \sim e^{-B\Delta t}$  for all  $\Delta t$ .  $B \approx 0.11$  for all  $f$ , whereas  $A = 0.055, 0.05$ , and  $0.043$  for  $f = 0.25, 1$ , and  $2$ , respectively, when  $N = 200$ . So, the proportion of events taking a longer time increases with  $f$ , which is in keeping with Fig. 1(b) where the proportion of long-segment events are seen to increase with  $f$ . This explicitly shows the weak increase of the characteristic correlation length with increasing  $f$ . The exponential decay  $n_E \sim e^{-A\Delta t}$  is slightly slower for polymers of length  $N = 100$  than of  $N = 200$ , see the plots for  $f = 2$  in Fig. 2. The dependence of  $A$  on  $N$  even for the maximum pore force  $f = 2$  is weak compared with its dependence on  $f$  and hence is not expected to have any effect on the scaling  $\tau \sim N^\alpha$ . The maximum event times and segment lengths are seen to increase only weakly with  $f$ . In summary, the form of the distribution of events with event time varies slightly with  $f$  and  $N$  for events toward *trans* but stays unaltered for events toward *cis*.

### D. Distributions for constant segment lengths

For DNA sequencing the important information is the time  $\Delta t$  it takes a polymer to traverse a distance  $\Delta s$  through the pore. Accordingly, we define  $t_E(\Delta s)$  as the total elapsed time for transitions of constant distance  $\Delta s$ .  $t_E$  consists of multiple separate events that take slightly different times  $\Delta t$ . We denote the number of such events  $n_E(\Delta s_{\text{const}}, \Delta t)$ . The total time spent on transferring segments of length  $\Delta s_{\text{const}}$  is thus  $t_E = \sum n_E(\Delta s_{\text{const}}, \Delta t) \cdot \Delta t(\Delta s_{\text{const}})$ , where the sum runs over all registered  $\Delta t$  for  $\Delta s_{\text{const}}$ . In Fig. 3 we show  $t_E$  for all registered discrete constant values of  $\Delta s$ . In what follows we omit the sub text 'const' from  $\Delta s$ . The obtained distributions are of the form

$$P(t_E(\Delta s)) \sim \frac{1}{\Delta s} \exp[-\ln(\Delta s/\Delta s_0)^2/2\sigma^2] \exp(-\Delta s/\Delta s_c), \quad (6)$$

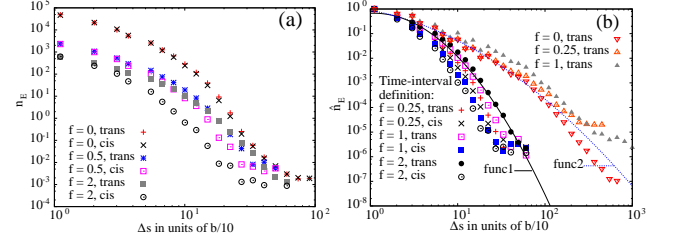


FIG. 1. (Color online) Log-binned distributions of events as sorted by the lengths of polymer segments that traverse in one direction, *trans* or *cis*, without pausing and sampled at time intervals, or without reversing for different pore force magnitudes  $f$ . The length of the polymer for all curves is  $N = 200$ . (a) The number of events  $n_E$  vs. segment length  $\Delta s$ .  $n_E$  is an average of numbers of events over several polymer translocations. (b) The numbers of events normalized with the maximum,  $\hat{n}_E = n_E/n_{\max}$  to compare the distributions. All distributions follow closely log-normal forms. The log-normal functions plotted to guide the eye are  $\text{func1} = 1/\Delta s * \exp(-\log(\Delta s/2)^2/1.2)$  and  $\text{func2} = 1/\Delta s * \exp(-\log(\Delta s/2)^2/4)$ . The apparent power-law decay at  $\Delta s > 300$  is an artefact due to the log-binning done on very few points there.

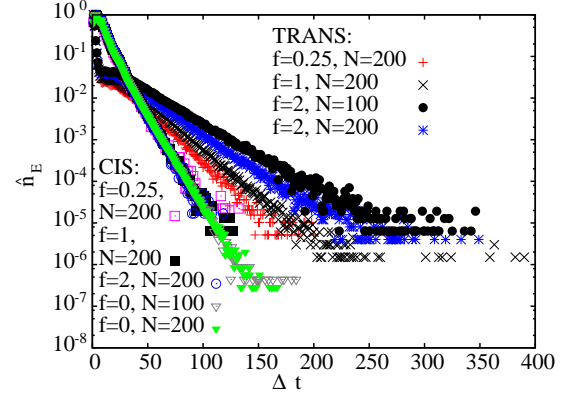


FIG. 2. (Color online) The event-time distributions  $n_E$  normalized with the maximum number of events. Semi-log scale shows the exponential decays. See the text for details.

where  $\Delta s_c$  is a finite cut-off. All these distributions can be fit by keeping  $\Delta s_c$  and  $\Delta s_0$  constant and varying  $\sigma$  in the log-normal part. The distribution data show fluctuations at small  $\Delta s$ , so we show cumulative distributions for improved quality. For a continuous variable  $x$  the cumulative distribution  $CP$  of the original distribution  $P$  is defined as  $CP(x) = \int_{-\infty}^x P(x)dx$ . So, for the discrete variable  $\Delta s$  we have  $CP(t_E(\Delta s)) = \sum_{\Delta s' = -\infty}^{\Delta s} P(t_E(\Delta s'))$ . Naturally, all these distributions can be fit with the cumulative form

$$CP(t_E(\Delta s)) \sim 1 - \text{erf}[\sqrt{\ln(\Delta s/\Delta s_0)^2/2\sigma^2 + \Delta s/\Delta s_c}]. \quad (7)$$

Again, the fits can be made by keeping  $\Delta s_c$  and  $\Delta s_0$  constant and varying  $\sigma$ , which increases with the pore force  $f$ . Unlike for the unforced translocation, for the forced translocation the broader cumulative log-normal distributions can also be fit with a decreasing power law and an exponential cutoff,  $\Delta s^{-\beta} \exp(-\Delta s/\Delta s_{co})$ .

The translocation times can be read off from the maximum

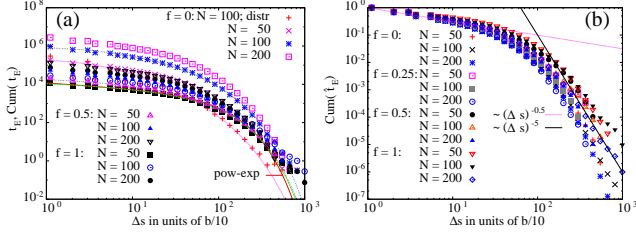


FIG. 3. (Color online) (a) The distribution (distr) of event times  $\Delta t$  with segment lengths  $\Delta s$  for  $f = 0$  and  $N = 100$ . The rest are cumulative distributions for  $f = 0, 0.5$  and  $1$ ,  $N = 50, 100$ , and  $200$ . The cut-off segment length  $\Delta s_c = 95$  and the characteristic scale  $\Delta s_0 = 6$  for all fit functions. The dispersion  $\sigma = 2, 7$ , and  $9.5$  for  $f = 0, 0.5$ , and  $1$ , respectively. Also shown is a fit with the function  $\text{pow-exp} \sim \Delta s^{-0.3} \exp(-\Delta s/60)$  for the cumulative distribution for  $f = 1$  and  $N = 50$ . (b) The cumulative distributions of (a) normalized by the maximum value. Lines  $\sim (\Delta s)^{-0.5}$  and  $\sim (\Delta s)^{-5}$  are drawn to guide the eye.

values of the cumulative distributions. Statistics is not as good as when  $\tau$  is directly measured from and averaged over individual simulations. The exponent values  $\alpha$  obtained this way are  $\alpha \gtrsim 2.2$  for  $f = 0$ , and  $\alpha \approx 1.4, 1.4, 1.45$  for  $f = 0.25, 0.5, 1$ , respectively. These approximative values are in keeping with our previous results and reported values for  $\alpha$  in general. The same values for  $\alpha$  are obtained by direct measurements of  $\tau$ , so this also verifies that the distributions were obtained correctly. The dependence of  $\alpha$  on  $f$  is mild compared to some of our earlier simulations. This may be caused by our more refined way of taking care that the pore force stays strictly constant, see Subsection II C. The effect of fluctuating pore force will be investigated in more detail in a forthcoming publication.

It is noteworthy that for the unforced and forced translocation there is a common constant cutoff length  $\Delta s_{co} \approx 95$  that does not increase with the pore force or change with the polymer length  $N$ . The proportion of traversed longer segments, however, increases with  $f$ , which is seen as a broadening of the log-normal distribution. Again, the form of the distribution changes very little with  $f$  or  $N$ , which can be more clearly seen from the normalized distributions in Fig 3(b). It would be tempting to think that the scaling  $\tau \sim N^\alpha$  resulted from the broad log-normal distribution of event times  $t_E(\Delta s)$ . However, the exponent values of the power-law segments  $(\Delta s)^{-0.5}$  and  $(\Delta s)^{-5}$  in Fig 3(b) do not give the correct scaling for  $\tau$ .

### E. How the scaling $\tau \sim N^\alpha$ comes about

To more precisely determine the role of events at different length scales we extract events of three different segment lengths  $\Delta s = 1, 10$ , and  $50$ . Extracting only the transitions of these three lengths  $\Delta s$  we obtain distributions of the total time  $t_E(\Delta s)$  depicting the contribution of different individual transition times  $\Delta t$ . These distributions are shown for pore force magnitudes  $f = 0$  and  $0.25$  in Fig. 4(a). The times taken up by events of  $\Delta s = 1$  are orders of magnitude larger than by events  $\Delta s = 10$  or  $50$  for all  $f \in [0, 2]$ . The peaks

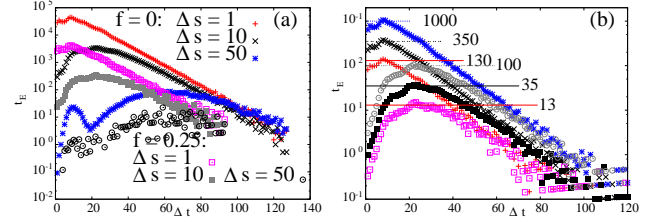


FIG. 4. (Color online) (a) Distributions of total time  $t_E$  for constant  $N = 200$  for transferred segment lengths  $\Delta s \in \{1, 10, 50\}$  and pore force values  $f = 0$  and  $0.25$ . (b) The distributions for the constant pore force  $f = 1$  and different polymer lengths  $N$ . The bottom three curves with maxima 13, 35, and 100 are for  $\Delta s = 10$  and  $N \in \{50, 100, 200\}$ . The topmost three curves with maxima 130, 350, and 1000 are for  $\Delta s = 1$  and the same polymer lengths. The marked maxima give the correct scaling  $\tau \sim N^\alpha$ , see the text.

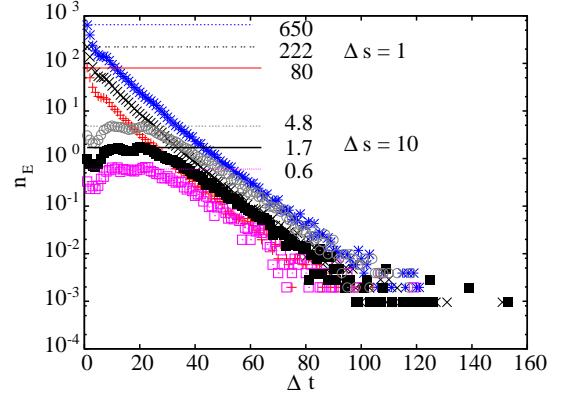


FIG. 5. (Color online) The distributions of the numbers  $n_E(\Delta s, \Delta t)$  for  $\Delta s = 1$ , and  $10$  for pore force  $f = 1$ . The indicated maxima give  $\alpha \approx 1.5$ .

in the range  $\Delta s \in [0, 20]$  most clearly visible for  $f = 0$  are due to the contribution of events toward *cis*. With increasing  $f$  this contribution diminishes for  $\Delta s = 10$  and  $50$  but not for  $\Delta s = 1$ . This partly explains the dominant contribution of very short transitions to the translocation time. For all  $f$ , almost all the contribution to  $\tau$  comes from events of small  $\Delta s$  and  $\Delta t$ . As  $\Delta t$  increases,  $t_E$  for different  $\Delta s$  approaches the same value.

The forms of the distributions  $t_E(\Delta s)$  for constant  $\Delta s$  are identical for all  $f$ , including  $f = 0$ . The maximum values of  $t_E$  for  $f = 0.25, 0.5$ , and  $1$  are  $\max(t_E) = 360, 180$ , and  $105$ , respectively, when  $\Delta s = 10$ , and  $\max(t_E) = 4200, 2100$ , and  $1050$ , respectively, when  $\Delta s = 1$ . These values give the scaling  $\tau \sim f^{-\beta}$  with  $\beta = 1$  for  $\Delta s = 1$  and  $\beta \lesssim 1$  for  $\Delta s = 10$ . Fig. 4(b) shows that maximum values of  $t_E(\Delta s)$  with  $\Delta s = 1$  or  $10$  give the scaling  $\tau \sim N^\alpha$ , where  $\alpha \approx 1.5$ . Since the distributions maintain their form, the numbers of events  $n_E(\Delta t)$  for constant  $\Delta s$  should give the same scaling as the total event times  $t_E$ . In Fig. 5 the event time and number distributions for  $f = 1$  and  $\Delta s \in \{1, 10\}$  are shown. The indicated maxima for the number distributions indeed give  $\alpha \approx 1.5$  just as the maxima for  $t_E$  distributions indicated in Fig. 4(b).

A more accurate estimate for  $\alpha$  can be obtained by summing up all the total event times or total event numbers for a constant  $\Delta s$ . These give for  $\Delta s = 1$ :  $\alpha = 1.45, 1.45$ , and  $1.47$  for  $f = 0.25, 0.5$ , and  $1$ , respectively; for  $\Delta s = 10$ :  $\alpha = 1.45, 1.44$ , and  $1.44$  for  $f = 0.25, 0.5$ , and  $1$  are obtained, respectively. From the direct measurement of the times it takes polymers to translocate we obtain  $\alpha = 1.45, 1.45$ , and  $1.47$  for  $f = 0.25, 0.5$ , and  $1$ , respectively. These are exactly the same values as obtained from the distributions for  $\Delta s = 1$ . The statistics for  $f = 0.25$  is rather modest, since for such a small pore force a vast majority of the simulated polymers slide back to the *cis* side without translocating. Even so, exactly same estimates for  $\alpha$  are obtained by the direct measurement of  $\tau$  and by summing up all  $t_E(\Delta s = 1)$ . The number of short range and time events determine the polymer translocation even for strongly driven translocation, and the effect of mildly changing forms of distributions is negligible.

#### IV. CONCLUSION

In conclusion, we have characterized the stochastic polymer translocation process with high length resolution. Our extensive simulations show that although the unforced and forced translocation processes are fundamentally different, the pertinent distributions are almost identical in form. The obtained log-normal forms of the event distributions suggest that both processes can be characterized as multiplicative stochastic processes. The out-of-equilibrium nature and the fact that the polymer segment transition probability through the pore varies with the process state, *i.e.* the position of the polymer with respect to the pore, also fit the general description of multiplicative processes.

Despite the strong non-equilibrium character of forced polymer translocation, the variation of scaling exponents in the relations  $\tau \sim N^\alpha$  and  $\tau \sim f^{-\beta}$  do not follow from *e.g.* the pore force changing the pertinent distributions but merely from different numbers of events taking place at a fraction of the length scale of the model monomer length. Consequently,

the noise contribution of the thermal heat bath remains significant in spite of the polymer being increasingly lifted out of it during the translocation process. The random fluctuations due to the heat bath restrict the lengths of the individual transitions of the polymer segments inside the pore. The random stochasticity exerted upon the segments inside the pore result from both the random force exerted directly on these segments and the random force resulting from the interaction of the dynamically changing polymer conformations and the heat bath outside the pore. Although we have shown that scaling of short transition events give the scaling of the whole polymer translocation, the reason for the scaling of the numbers of short transition events remains unsolved.

As we have shown previously, the most discernible conformational changes are the straightening of the polymer on the *cis* side and the crowding of the polymer segments on the *trans* side [7, 8]. These changes can be described in a coarse-grained fashion even if the stochasticity is omitted. However, the data presented here confirms that in spite of its strong out-of-equilibrium character the polymer translocation is essentially a driven diffusion process when dealing with pore force of realistic magnitude. The reported results also show the difficulty of controlling the exact position of the polymer inside the pore. Although the average translocation can be described in a coarse-grained manner based on force balance, it will not be of much avail in keeping a polymer segment fixed inside the pore. This enhances the importance of the ability to precisely control the pore-polymer interaction. This interaction should dominate over the stochastic fluctuations contributing to the random movement of the polymer inside the pore if nanopores are to be used for DNA sequencing.

#### ACKNOWLEDGMENTS

The computational resources of CSC-IT Centre for Science, Finland, are acknowledged.

- 
- [1] J. J. Kasianowicz, E. Brandin, D. Branton, and D. W. Deamer, *Proc. Natl. Acad. Sci. U.S.A.* **93**, 13770 (1996)
  - [2] W. Sung and P. J. Park, *Phys. Rev. Lett.* **77**, 783 (1996)
  - [3] M. Muthukumar, *J. of Chem. Phys.* **111**, 10371 (1999)
  - [4] J. Chuang, Y. Kantor, and M. Kardar, *Phys. Rev. E* **65**, 011802 (2001)
  - [5] Y. Kantor and M. Kardar, *Phys. Rev. E* **69**, 021806 (2004)
  - [6] T. Sakaue, *Phys. Rev. E* **76**, 021803 (2007)
  - [7] V. V. Lehtola, R. P. Linna, and K. Kaski, *EPL* **78**, 58006 (2009)
  - [8] V. V. Lehtola, R. P. Linna, and K. Kaski, *Phys. Rev. E* **78**, 061803 (2008)
  - [9] V. V. Lehtola, K. Kaski, and R. P. Linna, *Phys. Rev. E* **82**, 031908 (2010)
  - [10] J. Dubbeldam, V. Rostiashvili, A. Milchev, and T. Vilgis, *arXiv:1110.5763v1*(2011)
  - [11] T. Ikonen, A. Bhattacharya, T. Ala-Nissila, and W. Sung, *arXiv:1111.4782v1*(2011)
  - [12] V. V. Lehtola, R. P. Linna, and K. Kaski, *Phys. Rev. E* **81**, 031803 (2010)
  - [13] R. P. Linna and K. Kaski, *Phys. Rev. Lett.* **100**, 168104 (2008)
  - [14] D. Ermak and H. Buckholtz, *J. Comput. Phys.* **35**, 169 (1980)
  - [15] W. van Gunsteren and H. Berendsen, *Mol. Phys.* **34**, 1311 (1977)
  - [16] M. P. Allen and D. J. Tildesley, *Computer Simulation of Liquids* (Clarendon Press, Oxford, 2006)
  - [17] M. Wanunu, J. Sutin, B. McNally, A. Chow, and A. Meller, *Biophys. J.* **95**, 4716 (2008)
  - [18] B. Tinland, A. Pluen, J. Sturm, and G. Weill, *Macromol.* **30**, 5763 (1997)
  - [19] A. Meller, *J. Phys. Condens. Matter* **15**, R581 (2003)
  - [20] A. F. Sauer-Budge, J. A. Nyamwanda, D. K. Lubensky, and D. Branton, *Phys. Rev. Lett.* **90**, 238101 (2003)
  - [21] B. Luan and A. Aksimentiev, *Phys. Rev. E* **78**, 021912 (2008)
  - [22] S. van Dorp, U. Keyser, N. Dekker, C. Dekker, and S. G. Lemay,

- Nature Physics **5**, 347 (2009)
- [23] U. Keyser, B. Koeleman, S. Dorp, D. Krapf, Smeets, R., S. Lemay, N. Dekker, and C. Dekker, Nature Physics **2**, 473 (2006)
- [24] Y. Sasaki, H. Kuninaka, N. Kobayashi, and M. Matsushita, J. Phys. Soc. Jap. **76**, 074801 (2007)
- [25] S. Redner, Am. J. Phys. **58**, 267 (1990)
- [26] A. Schenzle and H. Brand, Phys. Rev. A **20**, 1628 (1979)
- [27] S. Havlin, B. Selinger, M. Schwartz, H. E. Stanley, and A. Bunde, Phys. Rev. Lett. **26**, 1438 (1988)
- [28] D. Sornette, *Critical Phenomena in Natural Sciences* (Springer-Verlag, Berlin Heidelberg, 2006)